Magnetic-field-induced sign reversal of transient photoreflectance in $Cd_{1-x}Mn_xTe$: Paramagnetic shift at low manganese concentration

W. Farah and D. Scalbert
Groupe d'Etude des Semiconducteurs, UMR5650 CNRS-Université Montpellier 2, Place Eugène Bataillon, 34095 Montpellier Cedex 5, France

M. Nawrocki
Institute of Experimental Physics, Warsaw University, Hoza 69, 00-681 Warszawa, Poland

Yu. G. Semenov
Institute of Semiconductor Physics, National Academy of Sciences of Ukraine, Prospect Nauki 45, Kiev, 252028, Ukraine
(Received 8 December 1997; revised manuscript received 27 March 1998)

Two thermomagnetic modulation mechanisms were revealed in photoreflectance modulation spectroscopy of $Cd_{1-x}Mn_xTe$ at low temperature. One is the thermal modulation of the magnetic redshift (paramagnetic shift) of the gap, the other is the magnetic-field-induced thermal modulation of the so-called giant spin splitting of the free exciton. In Faraday configuration and σ^+ polarization, these two magnetic contributions cancel each other for a particular magnetic field B_c. This causes a sign reversal of the photoreflectance signal around B_c. Analysis of the sign reversal is proposed as a tool for studying the paramagnetic shift at manganese concentrations x much lower than those reported so far. By using a model of the paramagnetic shift that takes into account interferences between Bloch waves scattered by spin-correlated ions, we obtain a good agreement with experimental results for x between 0.015 and 0.05. These interferences are shown to reduce the paramagnetic shift. For the lowest concentration studied this reduction amounts to a factor of approximately 1.7.
[S0163-1829(98)04528-7]

I. INTRODUCTION

The so-called diluted magnetic semiconductors (DMS's), generally II-VI compounds where a fraction of the cations are substituted by magnetic ions, have attracted a long-standing interest because of their specific magneto-optical properties.[1] These properties result from the strong sp-d exchange interactions between the band electrons and the magnetic ions. These exchange interactions are also known to produce a redshift of the fundamental gap of the semiconductor.[2,3] This redshift was first studied in magnetic semiconductors.[4] In II-VI DMS's the coupling between magnetic ions is antiferromagnetic and the redshift increases with temperature. The observed magnetic redshift, also called the paramagnetic shift (PS), could be accounted for by a term proportional to the magnetic fluctuations $bT\chi(T)$ where b is a constant for a given compound, T is the temperature, and $\chi(T)$ is the magnetic susceptibility.[2,3] In previous studies, the PS could be estimated only for relatively high magnetic ion concentrations ($x \geqslant 10\%$) by measuring the variations of the energy gap with temperature.

In this article we propose a method based on transient photoreflectance (TPR) spectroscopy in order to investigate the PS at much lower concentrations and at low temperature. We find that the PS is smaller than what is predicted by the simple expression given above and attribute this reduction to the appearance of long-range spin-spin correlations. In support of this interpretation we propose a model that takes into account the interferences between the Bloch waves scattered by spin-correlated ions.

In photoreflectance (photomodulated reflectivity) of non-magnetic semiconductors the light-induced reflectivity modulation is normally caused by that of the built-in surface electric field due to the photocarriers. In DMS's one may expect new modulation mechanisms of magnetic origin because the magnetic state is known to strongly influence the energy of optical transitions. Previous works using photoreflectance did not consider this possibility.[5,6]

Recently[7] we have proposed TPR for studying magnetic relaxation in $Cd_{1-x}Mn_xTe$ and demonstrated two thermomagnetic modulations: the modulation of the PS and that of the giant spin-splitting of the free exciton (i.e., the modulation of effective g factors). Transient reflectivity also indicated the possibility of PS modulation.[8] In these experiments a pump beam causes an increase of the manganese spin temperature and thus changes the PS and the giant spin splitting. These variations are then detected by measuring the reflectivity with a probe beam. For a well-chosen configuration of the probe beam (Faraday configuration and σ^+ circular polarization), as shown later, these thermomagnetic modulations give rise to a magnetic-field-induced sign reversal of TPR. This sign reversal occurs at a particular value of the field B_c, the magnitude of which is governed by the two competing modulations. The expression for the effective g-factor modulation being well known, the measurement of B_c provides direct information on the PS modulation. The sensitivity of the method allowed us to extend studies of the PS to situations where the magnetic ion content is as low as 1.5% at the superfluid helium temperature.

The paper will be organized as follows. In Sec. II the experimental setup is described. In Sec. III we concentrate on the discussion of the thermomagnetic modulation mecha-

nisms specific to DMS. In Sec. IV two methods are proposed for measuring the crossing field B_c. Section V is devoted to the comparison between the experimental results and predictions. The standard PS model of Refs. 2 and 3 is shown to be inadequate for describing the PS at low temperature and low concentration. A new model is put forward and provides a good agreement with the measured crossing field. A brief summary and conclusion are presented in Sec. VI.

II. EXPERIMENTAL DETAILS

We have performed experiments on bulk $Cd_{1-x}Mn_xTe$ crystals and on thick epilayers grown on GaAs substrates, with concentrations x in the range 1.5–5 %. The TPR was measured by means of a pump-probe optical setup. The sample was illuminated by two laser beams, one from an all-lines Ar^{2+} laser (pump), the second from a Al_2O_3:Ti tunable laser (probe). The two beams were directed towards synchronized acousto-optic modulators, which provided light pulses adjustable in width, 1–5 μs for the pump beam, and 20–200 ns for the probe beam, frequency ($f \sim 10$ kHz), and relative delay (0–10 μs), with a typical rise time of 10 ns. The time resolution of the experiment depends on the width of the probe pulses. The delay was electronically controlled. The pump beam with maximum peak intensity of about 15 W/cm^2 was unfocused, whereas the probe beam with mean power of about 25 μW was focused and superimposed on the pump spot.

The probe beam reflected by the sample was directed on a silicon photodetector through a diaphragm, neutral, and red filters. This ensured that luminescence or stray light from the pump beam be completely rejected. The pump beam was modulated at low frequency and phase-sensitive detection yielded the TPR signal. The reflectivity was obtained by measuring the dc photocurrent. The offset due to the photodiode dark current was carefully eliminated. The low-frequency modulation of the pump beam was produced electronically by using a gating facility of the (pump) pulse generator. This improved the signal over noise ratio. A positive TPR signal corresponded to an increase of reflectivity when the pump is on. The acquisition could be accomplished at a fixed delay as a function of the probe energy or at a fixed energy as a function of the delay. The experiments were performed in superfluid helium, at $T = 2$ K, and in Faraday configuration.

III. THERMOMAGNETIC MODULATIONS AND SIGN REVERSAL

In Ref. 7 it was shown that in $Cd_{1-x}Mn_xTe$, at low temperatures, the photoreflectance is mainly caused by two thermomagnetic modulation mechanisms: the thermal modulation of the PS and the thermal modulation of the effective giant spin splittings (i.e., modulation of effective g factors).

The PS modulation was identified on the basis of the fact that the relaxation time of the zero-field TPR signal agrees with that of the spin-lattice relaxation of Mn^{2+} ions. The sign of TPR in zero magnetic field is negative at the free-exciton resonance as expected for a redshift under illumination (see Figs. 1 and 4).

When the modulation of the effective g factors dominates, we expect one sign of the TPR or the other depending on whether the circular polarization of the probe beam is left handed or right handed. This property also provides an identification of this spin-dependent modulation mechanism. In σ^+ polarization the PS modulation and the g-factor modulation have opposite contributions. Hence, there exists a particular magnetic field B_c for which these two energy modulations cancel each other. As a consequence, the sign of TPR changes when the field crosses this value.

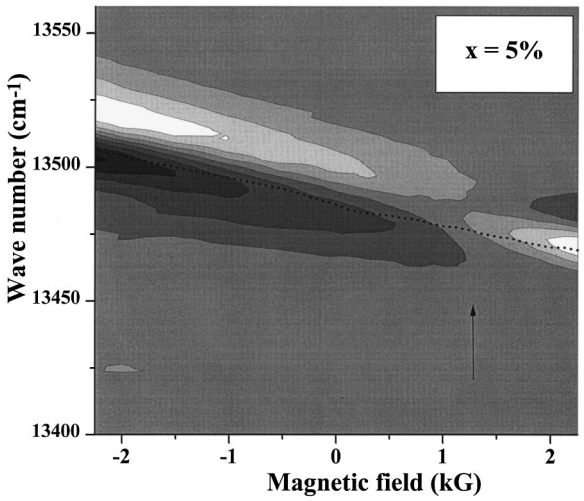

FIG. 1. Contour plot of transient photoreflectance $\Delta R/R$ in the plane (wave number, magnetic field) recorded at 2 K in Faraday geometry and at a constant delay (probe pulse at the end of the 5-μs-long pump pulse). Dark (bright) areas correspond to negative (positive) signal. The levels are equally spaced (1.5×10^{-3}). Positive (negative) fields correspond to σ^+ (σ^-) polarization and the overall slope is due to the Zeeman shift. The dotted curve shows the position of the excitonic resonance.

This sign-reversal phenomenon is illustrated in Fig. 1 by a contour map of TPR in the plane (magnetic field, wave number). The position of the strong exciton component measured at the inflection point of the reflectivity is indicated by the dashed line. In Fig. 1 the half-plane $B<0$ ($B>0$) corresponds to the σ^- (σ^+) circular polarization. From this contour map the magnetic field B where the sign reversal occurs can be estimated, as indicated by the arrow on the map. However a residual signal still persists at this field value. The TPR signal does not vanish simultaneously at all wavelengths. This hints to the fact that a modulation different from energy modulation must be present. The TPR lineshape fitting in Sec. IV indicates an oscillator strength modulation.

For the extremely diluted samples the decay of the TPR signal generally exhibits a long-living component, not influenced by the magnetic field. Nonmagnetic modulations can also contribute to the signal. Experiments done on pure CdTe, used as a reference sample, revealed simultaneously a very fast component (not resolved with our time resolution) and a long-living one. The modulation of the surface electric field[9] (typical in nonmagnetic semiconductors)[10] or the photorefractive properties of CdTe (Ref. 11) may be responsible for this signal. We have not studied yet in detail these mechanisms. Nevertheless, they can still be distinguished from the thermomagnetic modulations by analyzing the re-

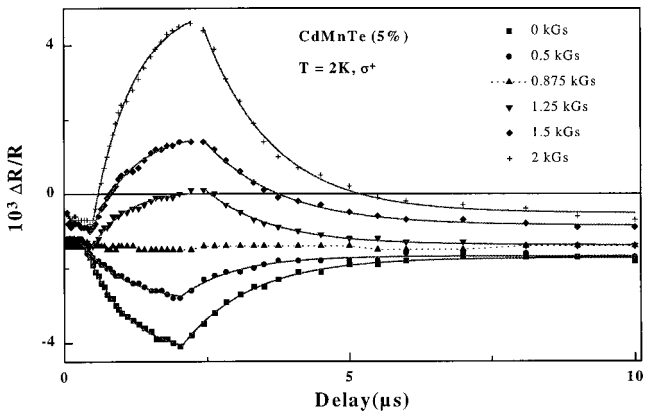

FIG. 2. Time dependence of photoreflectance for different magnetic fields recorded at the peak of TPR spectrum in σ^+ polarization. The solid lines are exponential fits to the data, the dotted line is a guide to the eye.

laxation time of the TPR signal.

Additionally, we have elucidated the effect of the pump intensity. The TPR signal is found to increase sublinearly with the pump intensity, indicating a sublinear increase of the temperature. Our analysis allows us to state that this behavior is not due to the variation of the heat capacity but rather to the variation of the Kapitza resistance (thermal boundary resistance) with the temperature.[12] This is normally expected in a steady-state regime where the increase of temperature at the sample surface is determined by the balance of heat fluxes. We find that the Kapitza resistance behaves approximately as T^{-3}, in agreement with predictions based on the acoustic mismatch model.[13] This result is also in favor of thermal modulations as being the leading effect in the present circumstance.

IV. DETERMINATION OF THE CROSSING FIELD

We define the crossing field B_c as the magnetic field for which the energy modulation of the strong exciton component $\Delta E=\Delta E_{\mathrm{PS}}+\Delta E_Z$ vanishes, ΔE_{PS} being the amplitude of the PS modulation and ΔE_Z that of the Zeeman shift modulation. Since we are dealing with thermal modulations we can write $\Delta E=(\partial E/\partial T)\Delta T$, where ΔT is the amplitude of the temperature modulation. Hence at the crossing field we must have $(\partial E_{\mathrm{PS}}/\partial T)=-(\partial E_Z/\partial T)_{B=B_C}$. This equality constitutes the central idea of the method proposed in this article in the study of the PS. Since the term on the right-hand side is well known, the determination of B_c provides directly the temperature derivative of the PS we are interested in. Note that the measurement of the zero-field TPR signal alone would give only access to ΔE_{PS}, but this does not allow us to evaluate $(\partial E_{\mathrm{PS}}/\partial T)$, as ΔT is not known *a priori*. Time-resolved measurements are also useful in order to discriminate the magnetic and possible nonmagnetic modulations.

We first focus on the determination of B_c by analyzing the time dependence of the TPR signal (Fig. 2). Each curve in Fig. 2 was obtained with the probe energy set at resonance with the free-exciton strong component for the σ^+ polarization (i.e., the probe was tuned along the dotted line of Fig. 1). This tuning was necessary in order to compensate the Zeeman shift. Moreover, this procedure allows us to reduce the possible effect of oscillator strength modulation, which does not contribute to the signal at the resonance.[14] The field-induced TPR signal due to the modulation of the spin splitting leads to a positive signal upon increasing B (Fig. 2). The relaxation time of the signal has been identified as being due to the spin-lattice relaxation of Mn^{2+};[7] it decreases with increasing Mn^{2+} concentration.[15] The zero-field signal exhibits the same relaxation time. This proves its magnetic origin which is attributed to the modulation of the PS. The flat curve at 0.875 kG corresponds to the field where the two contributions cancel each other (i.e., B_c). Note that at $B=B_c$ the signal does not vanish. This is due to the existence of a long living component (for this reason the field indicated by an arrow on Fig. 1 differs from B_c). We have repeated these experiments for samples with different concentrations. Note that because of the very nature of epitaxial layers, new lines are revealed below the free-exciton line; this is the consequence of the modulation of the optical path in these Fabry-Pérot-like samples.[16] These lines exhibit the same sign reversal as the exciton line and allow us to determine precisely the crossing field. The experimental values of B_c for both bulk samples and layers are summarized in Table I.

TABLE I. Calculated [Eq. (2)] and experimental crossing-field values expressed in kG for the different concentrations x investigated. T_0 and S_0 are the phenomenological parameters of the modified Brillouin function taken from Ref. 21 (a), or interpolated (b).

x (%)	T_0 (K)	S_0	B_c^{th}	B_c^{exp}
1.5 (layer)	0.81[b]	2.04[b]	1.02	0.31
2.0 (bulk)	0.94[a]	1.97[a]	1.19	0.50
3.2 (layer)	1.48[b]	1.79[b]	1.78	0.625
3.5 (bulk)	1.615[b]	1.75[b]	1.97	0.75
5.0 (bulk)	2.29[a]	1.54[a]	2.89	0.875

In what follows, we examine an alternative method for the determination of B_c. Given the fact that energy and oscillator strength modulations do not give rise to the same TPR line shape, it is worthwhile to investigate the TPR spectral evolution as a function of the magnetic field. In Figs. 3 and 4 we display the reflectivity and TPR spectra obtained for a series of magnetic field values and for $x=0.035$. The solid lines are fits to experimental data. For the fits of TPR data we assume that energy and oscillator strength modulations are the dominant factors. Calculations are done with the Seraphin formula.[17] For the dielectric function we use the following expression:

$$\varepsilon(E)=\varepsilon_b+f\sum_{j=0}^{1}\frac{1+2j}{4}\sum_{n=1}^{\infty}\frac{4}{n^3}\frac{E_R}{\gamma}\times\left[x_{nj}\Phi\left(\frac{1}{2},\frac{3}{2},\frac{x_{nj}^2}{2}\right)+i\sqrt{\frac{\pi}{2}}\right]\exp\left(-\frac{x_{nj}^2}{2}\right),$$

which includes contributions from bound exciton states and assumes a Gaussian broadening. ε_b is the background dielectric constant, f the oscillator strength, γ the broadening parameter, E_R the Rydberg of the exciton, E_{gj}'s the two band-gap energies for the strong ($j=1$) and weak ($j=0$) allowed

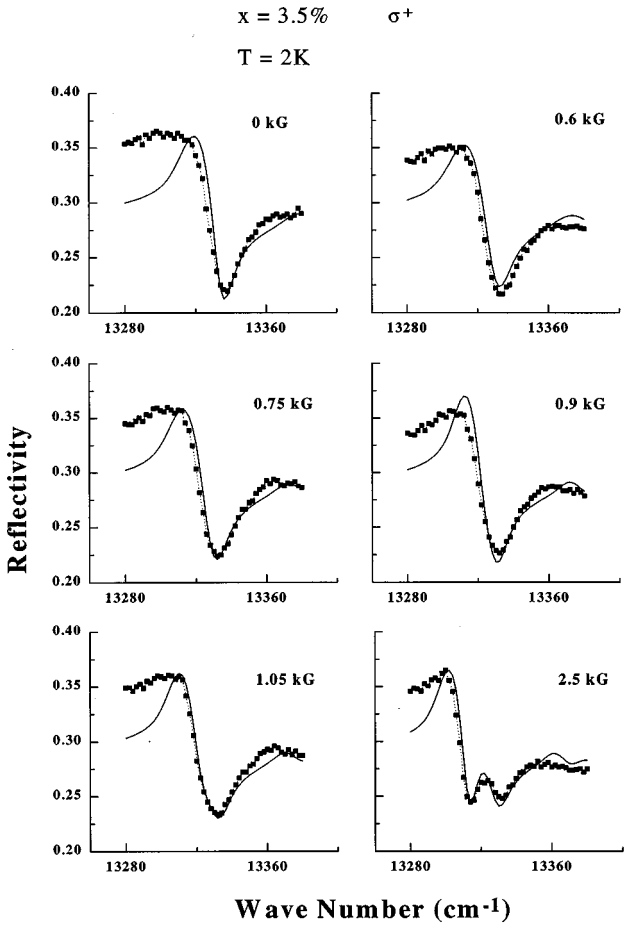

FIG. 3. Series of reflectivity spectra of $Cd_{0.965}Mn_{0.035}Te$ in Faraday configuration and σ^+ polarization, recorded with the probe pulse at the end of the pump pulse. Solid lines are fits to the data.

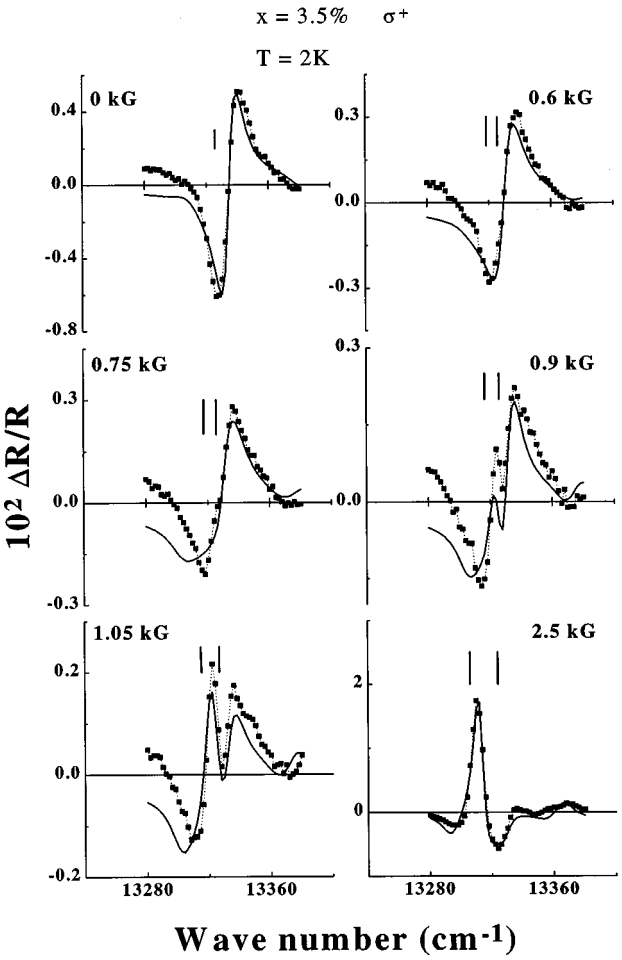

FIG. 4. Series of transient photoreflectance spectra of $Cd_{0.965}Mn_{0.035}Te$ in Faraday configuration and σ^+ polarization, recorded with the probe pulse at the end of the pump pulse. Solid lines are fitting to the data. The vertical lines indicate the energies of the two excitonic resonances.

optical transitions in σ^+ polarization, Φ the degenerate hypergeometric function,[18] and $x_{nj}=(E_{gj}-E_R/n^2-E)/\gamma$. We seek the best agreement between calculated and experimental results, both for the reflectivity and the TPR. First from fits of the reflectivity data we get $\varepsilon_b=10.88$ (Ref. 19) and $f=0.12$ (Ref. 20). γ varies from 8.4 to 6 cm^{-1} for increasing fields, while the E_{gj}'s behave as a function of the field according to the giant Zeeman shifts. Next, we introduce three modulation parameters for the fits of TPR data: modulations of E_{g0} and E_{g1} (ΔE_{gj}'s), and modulation of f (Δf). The TPR curves could not be reproduced, even qualitatively, if one of these modulations were omitted. The variations of the modulation parameters with the magnetic field are shown in Fig. 5. Within experimental errors the energy modulation of the strong exciton component ΔE_{g1} varies linearly, as expected, due to the modulation of the giant Zeeman splitting.

The line shape of TPR evolves in a complicated manner with the magnetic field. The line shape undergoes large changes for a restricted range of magnetic field values close to B_c (from 0.75 up to 1.05 kG), while reflectivity exhibits practically no change. The reasons are twofold. First, the existence of two close excitons components, which contribute comparably to TPR. Normally the contribution from the strong exciton component dominates over the weak one. In the vicinity of B_c, however, the energy modulation of the strong component tends to zero while that originating from the weak one remains finite. Second, close to B_c, the line shape also changes because oscillator strength modulation prevails against the energy one. The line shape analysis would be greatly simplified by lifting the zero-field degeneracy between light and heavy holes. This splitting occurs in wurtzite-type DMS's or in quantum wells. TPR studies in such systems would be very helpful in order to shed light on the physical origin of the oscillator strength modulation.

To improve the agreement between calculated and experimental results we have tempted to include a dead-layer effect. We were unable, however, to improve the fits of the reflectivity and TPR simultaneously. We were thus led to omit the dead-layer effect.

From these fits we obtained $B_c \approx 0.65$ kG, a value that is slightly smaller than that obtained with the first method for $x=0.035$. This result shows that the two methods are in good agreement. It must be emphasized, however, that the first method is more reliable. Indeed in one hand it allows us to distinguish between the magnetic and the nonmagnetic contributions, and, on the other hand, it does not depend on the choice of a particular model for fitting the experimental results.

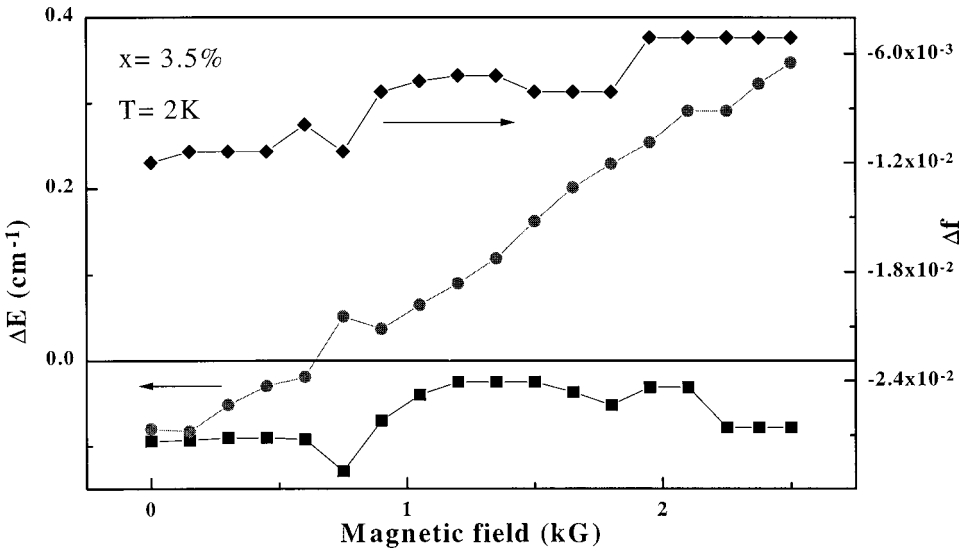

FIG. 5. Modulation parameters obtained from the fits shown in Fig. 4: energy modulation of strong (●) and weak (■) exciton components, oscillator strength modulation (◆).

The distinction between the magnetic and nonmagnetic parts becomes an essential task as the dilution increases, because so does the relative importance of the nonmagnetic contribution. Further experiments on samples with $x=0.005$ and $x=0.001$ have been performed. For $x=0.005$ the sign reversal of TPR occurs at a magnetic field much higher (above 5 kG) than the one expected for the pure magnetic modulations. For $x=0.001$ the sign reversal no longer exists, as for pure CdTe. These results can be explained by invoking the relative increase of the nonmagnetic modulation, which gives a negative signal. For these dilutions, in principle, the PS may be still investigated by TPR. However, our experimental setup is not suitable for the long relaxation times involved in this case. In what follows, we use the values of B_c obtained by analyzing the time dependence of the TPR signal, i.e., the first method, and for $x \geqslant 0.015$. These values are reported in Table I.

V. THEORETICAL MODELS AND COMPARISON WITH EXPERIMENTS

A. Incoherent phase model

We first evaluate B_c in the framework of existing models for the PS.[2,3] These models omit the phase factor, which appears in the spin-spin correlation function. In this approximation, the total magnetic shift of the low energy σ^+ transition reads

$$E_m=\frac{\beta-\alpha}{2g\mu_B}B\chi(T)+bT\chi(T), \tag{1}$$

where the first term is the Zeeman shift in the linear approximation and the second term is the PS according to Refs. 2 and 3. Due to the smallness of the magnetic fields considered here we have taken for the second term the zero-field expression of the PS. In this formula $\chi(T)$ is the temperature-dependent magnetic susceptibility, α and β are the exchange integrals for the conduction and valence bands. b is a parameter characteristic of a given host lattice; it has been found to be $b=-0.062$ eV G^2 erg^{-1} K^{-1} from the fitting of the temperature dependence of the band gap $E_g(T)$.[3] According to our definition B_c should obey $dE_m/dT=0$. Assuming $\chi(T)=C(x)/[T+T_0(x)]$ we find

$$B_c^{th}=b\,\frac{2g\mu_B}{\beta-\alpha}\,T_0(x). \tag{2}$$

As predicted by Eq. (2) $B_c^{\exp}$ increases with x (Table I). In Table I we have used the available values for $T_0(x)$ (Ref. 21) and a linear interpolation for other concentrations. If the zero-field TPR signal had a nonmagnetic origin, not dependent on x, we would then have expected a decrease of B_c with increasing x in contradiction with experimental results. This confirms the magnetic origin of the zero-field signal.

The experimental values are about twice as small as the calculated ones. This discrepancy originates most likely from the second term of Eq. (1), which is, valid neither at low temperatures nor at low concentrations.

In the following we propose a new model for evaluating the PS at low concentrations and at arbitrary temperature.

B. Model including the phase factor

Known models regarding the calculations of the PS (Refs. 2, 3, 22, and 23) are not appropriate neither for low magnetic ion concentrations nor at low temperatures. These models make use of the approximation that the nondiagonal part of the carrier-ion exchange interaction is of second order in perturbation. However, they disregard the effect of the interference factor (phase factor) in their perturbation theory. Here we will retain this factor. Most of the contribution to the PS comes from the exchange scattering inside the heavy-hole band. After some approximations,[23] the contribution to the hole energy at the center of the Brillouin zone takes the form

$$E^{(2)}=\tfrac{1}{4}(N_0\beta)^2x\,\frac{c}{N}\sum_{\mathbf{R}_j}\sum_{\mathbf{q}}\xi^2(\mathbf{q},0)\,\frac{\overline{\langle \mathbf{S}(\mathbf{R}_j)\mathbf{S}^1\rangle}}{E_{\mathbf{q}}}\exp(i\mathbf{q}\mathbf{R}_j), \tag{3}$$

where $\mathbf{R}_j$ is the position of magnetic ions with spins $\mathbf{S}(\mathbf{R}_j)$ and the origin is chosen at the site of spin $\mathbf{S}^1$, and $E_{\mathbf{q}}$ is the hole dispersion law. The summation on $\mathbf{R}_j$ extends over all cation sites occupied by a magnetic ion. The bar over the expression stands for averaging over all magnetic ion configurations. $\xi(\mathbf{q},0)$ represents the $\mathbf{q}$ dependence of the carrier-ion exchange integral.[3,23] The constant c stems from the projection of the heavy-hole state of the $\mathbf{k}\cdot\mathbf{p}$ Hamiltonian on the Γ_8 point: $c=\frac{1}{2}$ in the vicinity of Γ_8 (Ref. 23) and $c=0.51$ for larger wave vectors in the case of $Cd_{1-x}Mn_xTe$. Hence we took $c=0.5$ for all $\mathbf{q}$ in Eq. (3). N is the number of primitive cells in the pure crystal of volume V, $\langle\cdots\rangle$ denotes thermal averaging over the spin states.

In Refs. 2, 22, and 23 $E^{(2)}$ was estimated in two limits only: uncorrelated spins $[T\to\infty, \langle\mathbf{S}(\mathbf{r})\mathbf{S}\rangle\to\delta_{\mathbf{r},0}S(S+1)]$ and fully antiferromagnetic regime $[T\to 0, \langle\mathbf{S}(\mathbf{r})\mathbf{S}\rangle\to -S(S+1)$ for nearest-neighbor ions].

Gaj and Golnik[3] proposed to omit the phase factor $\exp(i\mathbf{qr})$ in Eq. (3) and expressed $E^{(2)}$ with the macroscopic magnetic susceptibility $\chi(T)$. They obtained a simple expression of the PS that we used in Eq. (1). However, that expression is valid in the high-temperature limit only, that is when spin-spin correlations are destroyed.

Below we show how antiferromagnetic spin-spin correlations influence the hole energy at finite temperature. The interferences between Bloch waves with finite $\mathbf{q}$ vectors scattered by spin-correlated ions are the principal physical effect introduced in our model.

We consider the very dilute limit when the average distance between nearest ions becomes longer than the range of the exchange interaction. In this case to a good approximation the sum over $\mathbf{R}_j$ in Eq. (3) can be restricted to the term corresponding to the nearest ion only. This approximation is similar to the extended nearest-neighbor pair approximation which was used in the interpretation of the magnetic properties of $Zn_{1-x}Mn_xSe$.[24] We note by r the distance of the nearest ion from the origin. Furthermore, we use the spherical approximation for the dispersion law and omit the term $R_j=R_1$ in Eq. (3). This term corresponds to a temperature-independent contribution in the total PS, which is not experimentally measurable. Note that this term and the temperature dependent term have opposite signs (cf. Appendix).

With the above approximations Eq. (3) takes the form

$$E^{(2)}=\frac{(N_0\beta)^2 xc\Omega_0}{8\pi^2 W}\int_0^{q_m}\xi^2(q,0)\,\overline{\frac{\sin qr}{qr}\,\langle\mathbf{S}(r)\mathbf{S}^1\rangle}\,\frac{q^2dq}{(E_q/W)}, \tag{4}$$

where W is the valence band width, $q_m=(6\pi^2/\Omega_0)^{1/3}$ is the maximum wave vector in the spherical approximation, and Ω_0 is the volume of the primitive cell. Now the bar denotes the averaging over r, the distance of nearest ion defined above.

The spin correlator $K(r)=\langle\mathbf{S}(r)\mathbf{S}^1\rangle$ was calculated using the exchange pair Hamiltonian,

$$H_{1,2}=-2J(r)\mathbf{S}_1\mathbf{S}_2+\omega_0 S_{1Z}+\omega_0 S_{2Z}. \tag{5}$$

Here J is the exchange constant for two ions with spins S_1 and S_2 and separated by r, $\omega_0=g\mu_B B$ is the Zeeman spin splitting. For $S=S_0=5/2$ straightforward calculations yield

$$K(r)=\frac{\sum_{F=0}^{5}\frac{1}{2}\left[F(F+1)-\frac{35}{2}\right](2F+1)\exp\left(\frac{F(F+1)J(r)}{T}\right)}{\sum_{F=0}^{5}(2F+1)\exp\left(\frac{F(F+1)J(r)}{T}\right)}, \tag{6}$$

where the temperature T is expressed in energy units, and F denotes the total spin of the pair. In the Appendix we show that the influence of interactions with other more distant spins can be taken into account by using an effective spin temperature $T+T_0$ instead of T in Eq. (6).

At low magnetic ion concentrations, the averaging over r in Eq. (4) can be evaluated in the continuous medium approximation, producing

$$E^{(2)}=\frac{(N_0\beta)^2x^2c}{2\pi W}\int_0^{\infty}I(a)K(a)\exp\left(-\frac{2}{9\pi}xa^3\right)a^2da, \tag{7}$$

$$I(a)=\frac{1}{a}\int_0^1\frac{\xi^2(z)\sin az}{E(z)/W}\,zdz, \tag{8}$$

where $z=q/q_m$ and $a=q_m r$.

In order to proceed further we must specify a dispersion law $E_q=E(z)$ and the spatial dependence of J. We assume

$$E_q=W[1-\cos(\pi q/2q_m)] \tag{9}$$

where W will be considered as a phenomenological parameter to be determined. For J we choose a power-law behavior[24] (see also Ref. 25 for a discussion on other laws proposed in the literature):

$$J=\begin{cases}J_0, & r<r_{12},\\ J_0\left(\frac{r_{12}}{r}\right)^k, & r>r_{12}.\end{cases} \tag{10}$$

Here J_0 represents the nearest-neighbor exchange constant and r_{12} is the distance between nearest neighbors. For $Cd_{1-x}Mn_xTe$ we used $J_0=-6.1$ K,[26] $r_{12}=4.58$ Å.[27]

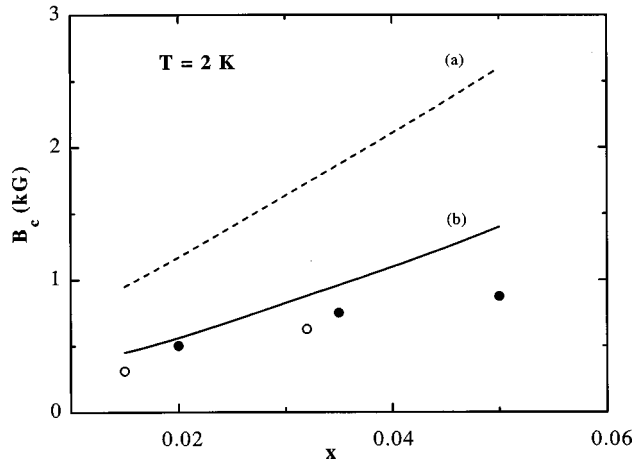

FIG. 6. Crossing field B_c vs molar fraction of Mn^{2+} content. The dashed line (a) corresponds to Eq. (2), which neglects the interference effects. The solid line (b) corresponds to Eq. (12), which includes the interference effects. The values measured on $Cd_{1-x}Mn_xTe$, taken from Table I, are given as open circles (layers) and close circles (bulk samples).

Finally, the following analytical approximation for ξ has been adopted:[23]

$$\xi(q,0)=\frac{1+q^2a_d^2/2}{(1+q^2a_d^2)^2}. \tag{11}$$

a_d is a length approximately equal to the d-shell radius. For $Cd_{1-x}Mn_xTe$ it was found that $a_d=1.37/q_m$.[23]

The above calculation of $E^{(2)}$ was implicitly done for zero magnetic field. In principle, the magnetic field would influence $E^{(2)}$ through the spin correlators and through the denominator, the energy E_q. However, our estimates show that for the small magnetic fields considered this influence is negligibly small.

We are in a position to evaluate the PS. This is accomplished by inserting the expressions of E_q, J, and ξ given by Eqs. (9)–(11) in Eq. (7). As before the crossing field B_c is obtained by requiring that the derivative of the total energy (Zeeman plus PS) be equal to zero. This leads to

$$B_c=-\frac{3x[N_0\beta(T+T_0)]^2}{\pi S_0(S+1)Wg\mu_B N_0(\beta-\alpha)} \times\int_0^\infty I(a)\,\frac{dK}{dT}\exp\left(-\frac{2xa^3}{9\pi}\right)a^2da. \tag{12}$$

All parameters in this expression are well known except for W and the exponent k introduced in Eq. (10). For the spin correlator K we used the effective temperature $T+T_0$ (see Appendix). To make a meaningful comparison with the models which neglect the interference factor, we require that the model should recover the values of B_c predicted by Eq. (2) when $\exp(i\mathbf{qr})\to 1$ [i.e., $I(a)\to I(0)$]. The next step is to look for the best agreement with experiments when the interference factor is included. These two conditions are best satisfied for $W=1.5$ eV and $k=7$. This value of k is very close to the exponent estimated for $Zn_{1-x}Mn_xSe$.[24] Figure 6 shows B_c evaluated in the both cases and the comparison with experimental values. We can see that the interferences reduce B_c by a factor about 2. The corresponding reduction of the PS is about 1.7 at the lowest concentration investigated here. Table II displays the values of $E^{(2)}$ calculated with Eq. (7). There we compare the two situations, namely the one where the interference factor is neglected, and the one where it is retained. The use of a quadratic dispersion law with a cutoff at $\frac{3}{4}q_m$ instead of the spherical approximation yields practically the same result.

TABLE II. Values of the paramagnetic shift $E^{(2)}$ calculated with Eq. (7) in two cases: when the interference factor (IF) is retained and when it is neglected. We took $W=1.5$ eV and $k=7$ deduced from the comparison between the experimental and calculated values of B_c (see text).

x (%)	$E^{(2)}$ (meV) (IF retained)	$E^{(2)}$ (meV) (IF neglected)
1.5	1.75	2.95
2.0	2.9	4.8
3.2	6.3	9.9
3.5	7.3	11.3
5	12.5	18.9

In Fig. 6 one can note that the disagreement between $B_c^{\rm th}$ (solid line) and $B_c^{\rm exp}$ increases with x. This is not surprising because our model uses an extended nearest-neighbor pair approximation, which is expected to be valid at low concentrations only.

VI. CONCLUSION

We have proposed a new method for investigating the PS in the dilute regime that is beyond the reach of conventional methods. Usually one measures the temperature dependence of the band gap in which the thermal expansion, the electron-phonon scattering, and the PS all give contributions. The absolute value of the PS cannot be measured separately. Similarly in our experiment only the derivative of the PS with respect to the temperature is accessible. The time resolution of the signal allows us to extract the magnetic contribution only.

We have obtained values of the crossing field B_c, which are about twice as small as those predicted by the standard PS formula. We have proposed a new model, which includes interferences between Bloch waves scattered by correlated spins. This phenomenon is shown to lead to a reduction of B_c and of the PS, and a satisfactory agreement with experimental results is obtained.

Furthermore, the experiments suggest that the oscillator strength modulation contributes to the TPR signal. Its physical origin, however, is at present not clear. Further investigations are necessary in order to identify the underlying modulation mechanism. In particular, TPR experiments performed on crystals with the wurzite structure or on DMS-based quantum wells are desirable. The preexisting splitting between light- and heavy-hole states, in those circumstances, would simplify the line-shape analysis and would offer the possibility to study separately the PS for each optical transition.

The study presented here was limited to low magnetic fields, but high enough to observe the crossing field (typi-

cally in the kG range) and to estimate quantitatively the PS. The high-field regime is, however, not devoid of interest. In the limit of very high magnetic fields the thermomagnetic modulations must be suppressed, since the magnetization saturates and the magnetic fluctuations are inhibited; only the nonmagnetic modulations would persist. However, in practice, very high magnetic fields are necessary to eliminate the magnetic fluctuations, especially the transverse ones. Also the validity of the theory presented above is limited to low magnetic fields, so that the present theory becomes questionable.

ACKNOWLEDGMENTS

This work was supported in part by Ukrainian Fundamental Research Grant No. 2.4/871. Part of the experimental results presented in this paper were obtained on epilayers grown at the Polish Academy of Sciences by T. Wojtowicz, G. Karcewski, and E. Janik. We thank C. Misbah for a critical reading of the manuscript.

APPENDIX

The magnetic susceptibility per spin S at zero magnetic field is determined from

$$\chi_0=\frac{(g\mu_B)^2}{3TN_m}\left\langle\left(\sum_j \mathbf{S}^j\right)^2\right\rangle. \tag{A1}$$

The sum is over all N_m magnetic ions, and therefore averaging over different possible magnetic configurations, will give the same result. The expression in brackets can be separated into two parts: the temperature-independent part, proportional to $\Sigma_j(\mathbf{S}^j)^2=N_mS(S+1)$, and the spin correlator $2N_m\Sigma_{j>1}\overline{\langle \mathbf{S}^1\mathbf{S}^j\rangle}$.

Now we can express this spin correlator in terms of the phenomenological parameters S_0 and T_0, using the modified Brillouin function for magnetization. After substitution of $\chi_0=1/3S_0(S+1)(g\mu_B)^2/(T+T_0)$ in left-hand side of Eq. (A1) we find

$$\sum_{j>1}\overline{\langle \mathbf{S}^1\mathbf{S}^j\rangle}=-S(S+1)\,\frac{(S-S_0)+ST_0/T}{S(1+T_0/T)}, \tag{A2}$$

where the position of the ion number 1 is fixed by the origin of the coordinate system, the other magnetic ions positions must be averaged.

We have compared the expression of the spin correlator (A2) with that calculated using Eq. (6) averaged over the shortest distances r, as defined in the text (within the extended nearest-neighbor pair approximation), for various concentrations and temperatures in the range 2–10 K.

We found a good agreement between the phenomenological and microscopic calculations. Nevertheless, a sizable deviation is obtained for $x=0.05$, the highest concentration studied here. In our opinion it means that the approximation used to calculate the correlator is no longer valid at this concentration.

We can try to consider the influence of fluctuating interactions with more distant ions in the microscopic calculation. For this purpose we propose to calculate the spin correlator in the spirit of the mean-field approximation by introducing an effective temperature $T_{\rm eff}=T+T_0$ instead of T in the correlator K. With this trick, the two methods now give practically identical results for all the magnetic ion concentrations considered.

[1] O. Goede and W. Heimbrodt, Phys. Status Solidi B **146**, 11 (1988); J. K. Furdyna, J. Appl. Phys. **64**, R29 (1988); R. K. Willardson and A. C. Beer, in *Semiconductors and Semimetals*, edited by J. K. Furdyna and J. Kossut, Diluted Magnetic Semiconductors (Academic, Boston, 1988), Vol. 25; *Semimagnetic Semiconductors and Diluted Magnetic Semiconductors*, edited by M. Averous and M. Balkanski (Plenum, London, 1991).

[2] R. B. Bylsma, W. M. Becker, J. Kossut, U. Debska, and D. Yoder-Short, Phys. Rev. B **33**, 8207 (1986).

[3] J. A. Gaj and A. Golnik, Acta Phys. Pol. A **71**, 197 (1987).

[4] G. Busch and P. Wachter, Phys. Kondens. Mater. **5**, 232 (1966); G. Harbeke and H. Pinch, Phys. Rev. Lett. **17**, 1090 (1966).

[5] J. Misiewicz, X.-L. Zheng, P. Becla, and D. Heiman, Solid State Commun. **66**, 351 (1988).

[6] Y. R. Lee, A. K. Ramdas, and R. L. Aggarwal, Phys. Rev. B **38**, 10 600 (1988).

[7] D. Scalbert, W. Farah, and M. Nawrocki, in *Proceedings of the 23rd International Conference on the Physics of Semiconductors*, edited by M. Scheffler and R. Zimmermann (World Scientific, Singapore, 1996), p. 433.

[8] W. Farah, D. Scalbert, and M. Nawrocki, Phys. Rev. B **53**, R10 461 (1996).

[9] M. P. Lisitsa, S. F. Terekhova, and G. G. Tsebulya, Fiz. Tekh. Poluprovodn. **8**, 1361 (1974) [Sov. Phys. Semicond. **8**, 883 (1975)].

[10] D. E. Aspnes, Solid State Commun. **8**, 267 (1967); R. E. Nahory and J. L. Shay, Phys. Rev. Lett. **21**, 1569 (1968); F. Cerdeira and M. Cardona, Solid State Commun. **4**, 879 (1969).

[11] R. B. Bylsma, P. M. Bridenbaugh, D. H. Olson, and A. M. Glass, Appl. Phys. Lett. **51**, 889 (1987).

[12] E. T. Swartz and R. O. Pohl, Rev. Mod. Phys. **61**, 605 (1989).

[13] I. M. Khalatnikov, Zh. Eksp. Teor. Fiz. **22**, 687 (1952).

[14] O. J. Glembocki and B. V. Shanabrook, in *Semiconductors and Semimetals*, edited by David G. Seiler and Christopher L. Littler, The Spectroscopy of Semiconductors (Academic, Boston, 1992), Vol. 36.

[15] D. Scalbert, J. Cernogora, and C. Benoit à la Guillaume, Solid State Commun. **66**, 571 (1988).

[16] W. Farah, D. Scalbert, M. Nawrocki, J. A. Gaj, E. Janik, G. Karczewski, and T. Wojtowicz, Phys. Rev. B **57**, 8770 (1998).

[17] B. O. Seraphin and N. Bottka, Phys. Rev. **145**, 628 (1966).

[18] H. Shen, S. H. Pan, Fred H. Pollak, M. Dutta, and T. R. AuCoin, Phys. Rev. B **36**, 9384 (1987).

[19] This value is slightly smaller than the static dielectric constant

$\kappa = 12.5$ reported by J. Jaroszynski and T. Dietl, Solid State Commun. **55**, 491 (1985).

[20] Using the obtained values of ε_b and f, the longitudinal-transverse splitting can be crudely estimated as $\Delta_{LT} \approx 4fE_R/\varepsilon_b \approx 0.44$ meV, which is in reasonable agreement with $\Delta_{LT} = 0.65$ meV determined by Brillouin scattering: J. C. Merle, R. Sooryakumar, and M. Cardona, Phys. Rev. B **30**, 3261 (1984).

[21] J. A. Gaj, R. Planel, and G. Fishman, Solid State Commun. **29**, 435 (1979).

[22] J. Diouri, J. P. Lascaray, and M. El Amrani, Phys. Rev. B **31**, 7995 (1985).

[23] S. M. Ryabchenko, Yu. G. Semenov, and O. V. Terletski, Phys. Status Solidi B **144**, 661 (1987).

[24] A. Twardowski, H. J. Swagten, W. J. M. de Jonge, and M. Demianiuk, Phys. Rev. B **36**, 7013 (1987).

[25] Qun Shen, H. Luo, and J. K. Furdyna, Phys. Rev. Lett. **75**, 2590 (1995).

[26] V. Bindilatti, T. Q. Vu, and Y. Shapira, Solid State Commun. **77**, 423 (1991).

[27] W. L. Roth, in *Physics and Chemistry of II–VI Compounds*, edited by M. Aven and J. S. Prener (North Holland, Amsterdam, 1967).